Assessment of soil moisture effects on L-band radar interferometry

Simon Zwieback [a,*], Scott Hensley [b], Irena Hajnsek [a,c]

[a] *Institute of Environmental Engineering, ETH Zurich, Zurich, Switzerland*
[b] *Jet Propulsion Laboratory, California Institute of Technology, Pasadena, CA, USA*
[c] *Microwaves and Radar Institute, German Aerospace Center (DLR), Wessling, Germany*

A B S T R A C T

Differential SAR interferometry, a popular technique for measuring displacements of the Earth's surface, is potentially influenced by changes in soil moisture. Different mechanisms for this impact have been proposed, but its magnitude, sign and even presence remain poorly understood. In this study the dependence of the phase, the coherence magnitude as well as the phase triplets on soil moisture was inferred empirically with regression techniques: this was done for two airborne data sets at L-band. The phase dependence was significant (at a significance level of 0.05) for more than 70% of the fields at HH polarization, its sign corresponding to an increase in optical path upon wetting, and the magnitude of the associated deformation commonly exceeding 2 cm for a change in soil moisture of 20%. This trend was similar in both campaigns, whereas the prevalence of soil moisture-related decorrelation differs. These results are only consistent with a dielectric origin of the soil moisture effects, and not with soil swelling or the penetration depth hypothesis. Changes in vegetation impact the phase depending on the crop and polarization, with the vegetation influence at VV being more pronounced for the agricultural crops present in the study area.

© 2015 The Authors. Published by Elsevier Inc. This is an open access article under the CC BY-NC-ND license (http://creativecommons.org/licenses/by-nc-nd/4.0/).

1. Introduction

Radar interferometry is an established technique for the observation of a broad range of phenomena. These include volcanology (Massonnet, Briole, & Arnaud, 1995), tectonics (Massonnet et al., 1993), permafrost studies (Liu, Zhang, & Wahr, 2010), or the analysis of groundwater-related subsidence (Galloway & Hoffmann, 2007). It works by coherently combining two radar images. When these images are acquired at different times, the technique is sensitive to displacements on the scale of the radar wavelength, i.e. typically 1–10 cm (Gabriel, Goldstein, & Zebker, 1989; Rosen et al., 2000). These two images can also be taken from different positions, in which case height information can be derived from the data (Bamler & Hartl, 1998).

When there is a time gap between the two acquisitions, not only can there be deformations, but also the vegetation and soil moisture can change. If this is the case, such soil moisture m_v changes can lead to systematic errors in the estimated deformations. However, the prevalence and magnitude of these influences are not well understood. A possible influence of variations in soil moisture on the interferometric signal was initially postulated by Gabriel et al. (1989) due to an observed correspondence of the phase ϕ and thus the estimated deformations with hydrological units such as agricultural fields. However, dedicated observational studies have been scarce and limited to a handful of laboratory experiments (Morrison, Bennett, Nolan, & Menon, 2011; Nesti et al., 1998; Rudant et al., 1996; Yin, Hong, Li, & Lin, 2014), as well as a few air- or satellite-borne campaigns (Barrett, Whelan, & Dwyer, 2012; Barrett, Whelan, & Dwyer, 2013; Hajnsek & Prats, 2008; Hensley et al., 2011; Nolan, 2003a). Simultaneously, different mechanisms and models that could describe some of these effects have been proposed, alongside electromagnetic simulations based on Maxwell's equations (Rabus, Wehn, & Nolan, 2010). These explanations attribute the change in ϕ to deformations (Gabriel et al., 1989), changes in the optical path due to soil moisture variations Δm_v (De Zan, Parizzi, Prats-Iraola, & Lopez-Dekker, 2014; Rudant et al., 1996), or differences in the penetration depth of electromagnetic waves (Nolan, 2003b).

Despite these analyses, there is no consensus on the magnitude, sign and even presence of these effects (Morrison et al., 2011; Rabus et al., 2010; Rudant et al., 1996). This is partly due to the lack of suitable data. The speckle patterns tend to decorrelate over time, which implies that the phase cannot be estimated reliably (Barrett et al., 2013; Zebker & Villasenor, 1992). The lack of temporal stability of many areas (especially those covered by vegetation) has led to the development of algorithms that estimate deformations using only stable, point-like scatterers (Ferretti et al., 2011). When the data over the less stable areas are to be analysed with respect to the influence of soil moisture on the phase, a small time gap and preferably bare soil are required. In addition, the radar signals are also influenced by other parameters such as the elevation (for non-zero spatial baselines), deformations,

* Corresponding author at: Stefano-Franscini-Platz 3, 8093 Zuerich, Switzerland.
Tel.: +41 44 633 34 04.
E-mail address: zwieback@ifu.baug.ethz.ch (S. Zwieback).

and vegetation properties. Furthermore, there are sizeable differences between the different studies with regards to the wavelength, incidence angle, soil type, vegetation cover, etc., and these render comparisons and model assessments difficult (Barrett et al., 2013). The proposed explanations have not yet been assessed with extended data sets or compared with each other.

In view of these open questions, we want to study these soil moisture effects in two L-band airborne campaigns. The low frequency, short revisit times, small spatial baselines, and (in one campaign) absence of vegetation cover are expected to reduce the impact of these additional influences such as the topography and vegetation-related processes. The soil moisture effects, by contrast, are expected to be more dominant and thus detectable. In particular, this allows us to address the question of the sign, magnitude and statistical significance of these effects. We do so by using regression techniques whereby we describe the interferometric observables as a function of the change in soil moisture Δm_v. Furthermore, we want to assess the plausibility of the different conjectured mechanisms that could describe these effects. This assessment is made by comparing their predictions with the empirically found impact of soil moisture on the interferometric data. As the applicability and relevance of these explanations are not well understood, we focus on the differences between these explanations rather than particular models and parameterizations. This analysis is conducted for different polarizations, as the sensitivity to soil moisture is not necessarily identical. In most previous studies (both observational and models), the polarimetric aspect was not addressed explicitly, often due to lack of suitable data or because the proposed physical explanations did not involve any polarimetric differences (De Zan et al., 2014; Nolan, 2003a).

The interferometric observables along with the notation and sign conventions of this paper are introduced in Section 2. Subsequently, the study sites and data sets are outlined, followed by an overview of the SAR processing and the statistical methods. The results of these analyses are presented in Section 6; in Section 7 they are scrutinized and compared to the predictions of the different hypotheses.

2. Radar interferometry

In a polarimetric framework (Cloude, 2009), from which the standard single channel scenario arises as a special case, each single look complex (SLC) pixel is described by a scattering vector $\mathbf{q}$; in the lexicographic basis (reciprocal backscatter situation), $\mathbf{q} = \left[S_{HH}, \sqrt{2}S_{HV}, S_{VV} \right]$. From two SLC images $\mathbf{q}_1$ and $\mathbf{q}_2$ – they usually differ in their acquisition time and/or position – one derives the scalar quantity called complex coherence (Cloude & Papathanassiou, 1998)

$$\gamma_{12}(\omega) = \frac{\omega^{\dagger}\left\langle \mathbf{q}_1\mathbf{q}_2^{\dagger} \right\rangle\omega}{\sqrt{\omega^{\dagger}\left\langle \mathbf{q}_1\mathbf{q}_1^{\dagger} \right\rangle\omega\, \omega^{\dagger}\left\langle \mathbf{q}_2\mathbf{q}_2^{\dagger} \right\rangle\omega}} \qquad (1)$$

where ω is a polarimetric measurement functional (e.g. $[1, 0, 0]^T$ for HH). The $\langle \cdot \rangle$ denotes an ensemble average, which can be estimated by spatial multilooking (Bamler & Hartl, 1998; Gabriel et al., 1989). This averaging applies if the target is treated as a distributed one, i.e. as realization of a random process. The coherence can be factored as $\gamma = |\gamma|exp(i\phi)$. From this factorization, the three observables (phase ϕ, coherence magnitude $|\gamma|$, and phase triplets Ξ) used in this study can be derived.

The phase ϕ (the $exp(i\omega t)$ convention is employed throughout) is sensitive to the geometry and displacements. After flat earth phase removal, spectral filtering, and neglecting noise and propagation effects in e.g. the atmosphere, ϕ of a point target can be approximated as $\phi = \kappa_z z + 2k_0 d$, where the first part determines the impact of the elevation above a reference surface z, and the second one to displacements d along the RADAR look direction. The first coefficient of proportionality is

given by $\kappa_z \equiv \left(\frac{\partial \phi}{\partial z} \right)_R \propto k_0 B_\perp R^{-1}$, where $B_\perp$ is the antenna offset perpendicular to the look direction, R the distance to the target, and k_0 the wavenumber in free space. The sensitivity to displacements is given by twice the wavenumber in free space.

The coherence magnitude $|\gamma|$ can be interpreted as a measure of the correlation of the speckle patterns in $\mathbf{q}_1$ and $\mathbf{q}_2$ (Rosen et al., 2000). A value less than one can e.g. be caused by volume scattering for $B_\perp \neq 0$, or by changes in the arrangement and physical properties of the target for non-simultaneous acquisitions, as well as noise (Tsang, Kong, & Ding, 2000).

The phase triplets (De Zan et al., 2014; Ferretti et al., 2011) are a combination of the phases of the three interferograms formed from three SLC images $\Xi_{123} = \phi_{12} + \phi_{23} - \phi_{13}$: they are only different from zero if $|\gamma_{ij}| \neq 1$. In astronomy they are usually referred to as closure phases (Monnier, 2007) and have proven useful due to their insensitivity to a phase offset (e.g. due to the atmosphere) in any of the acquisitions.

3. Hypotheses

The four hypotheses about the origins of the soil moisture effects that have been framed in the literature will each be briefly presented. The focus will be less on the implementation of these mechanisms in particular parameterized models, but rather on the physical basis and the predictions that can be formulated based on them. The sign of the dependence of the interferometric observables on soil moisture changes Δm_v for each of the mechanisms is summarized in Table 1. These explanations, although distinct, are not necessarily mutually exclusive.

3.1. Null hypothesis (Null)

The null hypothesis states that there is no relationship between the moisture content and the interferometric observables, including the phase ϕ; this is schematically depicted in Fig. 1a. This hypothesis is implicitly assumed in virtually all interferometric studies (Ferretti et al., 2011), where soil moisture effects are either not considered, minimized by excluding soil, or deemed negligible.

3.2. Deformation (Defo)

ϕ variations whose patterns match those of hydrological units such as field boundaries have previously been interpreted as deformations (Gabriel et al., 1989; Nolan, 2003a). Certain types of soils (e.g. montmorrillonite clay) are known to swell upon wetting (Mitchell, 1991; Norrish, 1954), and such deformations have indeed been studied (and compared with in-situ measurements) with differential interferometry (te Brake, Hanssen, van der Ploeg, & de Rooij, 2013). The influence of an expanding soil on the phase of the coherence is illustrated in Fig. 1b. The impact on the magnitude of the coherence depends intricately on the detailed mechanism: a piston-like shift would in general not lead to decorrelation, whereas non-uniform deformations easily could. The generality of these effects is, however, doubtful, as these swelling and shrinking behaviours are restricted to certain types of soil (Mitchell, 1991). Furthermore, the sensitivity of ϕ to these effects diminishes with decreasing radar frequency. For example, at L-band

Table 1

Model predictions for the sign of the sensitivity of an observable on m_v: + positive, − negative, 0 no influence, and ? not explicable. The volume hypothesis is used for the Diel mechanism.

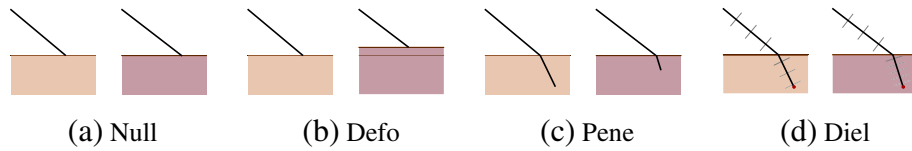|	Null	Defo	Pene	Diel
$\frac{\phi}{\Delta m_v}$	0	−	−	+
$\frac{|\gamma|}{|\Delta m_v|}$	0	0?	?	−
$\Xi(m_{v0\,:\,2})$	0	0	?	$\neq 0$

Fig. 1. Schematic depictions of the postulated mechanisms giving rise to the interferometric phase φ; left image: dry soil, right one: moist soil. A positive $\frac{\phi}{\Delta m_v}$ corresponds to an increase in the optical path upon wetting (e.g. due to subsidence).

$\phi = \pi$ corresponds to a deformation of about 5 cm, at X-band to 0.5 cm. Especially at such longer wavelengths, observed phase values that are of this magnitude have been deemed too large to be plausibly caused by deformations (Hensley et al., 2011).

3.3. Penetration depth (Pene)

Nolan (2003b) suggested that the penetration into the lossy soil governs the phase signal. When the soil is treated as a homogeneous uniform dielectric medium, the former can be parameterized in terms of the wavelength and the dielectric constant ε (the dependence on soil moisture is described in terms of a mixing model, e.g. (Mironov, Kerr, Wigneron, Kosolapova, & Demontoux, 2013)). The soil moisture content governs the characteristic length scale δ at which the wave attenuates (Tsang et al., 2000). According to the penetration depth hypothesis, the phase is then related to a difference in δ, cf. Fig. 1c. There are two inherent problems in this approach. Firstly, it is not clearly stated how the change in penetration depth is related to the observable φ: δ is a characteristic length, the scaling of which is somewhat arbitrary. Furthermore, in free space the propagation phase is related to the distance R by $\varphi = -2k_0 R$: in a dielectric medium the free-space wavenumber k_0 should be replaced by the one specific to this medium and frequency. It is not clear which conversion (Nolan, 2003b) apply. Secondly, the model does not predict the coherence $|\gamma|$. Indeed, it does not explain how a non-zero correlation can be achieved, as there is no physical mechanism postulated that could give rise to such correlations. One possibility in a non-uniform soil consisting of two layers with highly correlated rough surfaces was studied by Rabus et al. (2010) and shown to give rise to such a phase signal but also to be exceedingly sensitive to the geometrical parameters.

Let the penetration depth σ be defined to be the depth at which the two-way propagation at an incidence angle of 34° leads to reduction in power by a factor of $\frac{1}{e}$. At L-band the commonly used Hallikainen model predicts a value for σ of 2 cm for wet conditions of $m_v = 0.4$ m³ m⁻³, and 4 cm for dry conditions of $m_v = 0.1$ m³ m⁻³. The Peplinski model, for which the absorption in the soil is smaller (Hallikainen, Ulaby, Dobson, El-Rayes, & Wu, 1985; Peplinski, Ulaby, & Dobson, 1995), predicts in these conditions values of δ of 5 and 13 cm, respectively.

3.4. Dielectric mechanism (Diel)

The dielectric properties of a medium govern the complex wave vector k: an example applicable to DInSAR are changes in atmospheric properties that influence the measured φ. This idea was extended by Rudant et al. (1996) to the vegetation overlying the soil as well as the soil itself, as the dielectric properties of both are known to depend on the moisture content (Tsang et al., 2000). This effect has been observed (as well as modelled) for a buried reflector in a laboratory experiment (Morrison, Bennett, & Nolan, 2013); it can also be interpreted as the mechanism giving rise to the phase signal observed in a numerical electromagnetic model of an inhomogeneous soil (Rabus et al., 2010). De Zan et al. (2014) described the soil as an aggregate of such inhomogeneities and derived the first-order scattering solution of the coherence γ: the radar signal is thus modelled as the superposition of contributions from a large number of scatterers within the soil (surface scattering is

not considered). Note that non-zero phase triplets Ξ are predicted by this model.

Within the context of this first-order scattering model (FOSM), a change in the dielectric constant corresponds to a change in the wavenumber k in the medium: the real part of the latter encodes how rapidly the phase changes with position (the spacing of the wavefronts in Fig. 1d), the absorption with depth is governed by the imaginary part (the darkness of the wavefronts in Fig. 1d). Under the independent scattering assumption and if the positions of the inhomogeneities are uncorrelated, it is the real part that gives rise to a non-zero φ, conversely to the penetration depth approach (De Zan et al., 2014).

Even in the absence of inhomogeneities within the soil, a change in the dielectric properties is predicted to lead to phase changes by rough surface scattering models (assuming identical geometric properties for the two acquisitions). For sufficiently small wavelengths (compared to the radius of curvature and root-mean-square (RMS) height of the rough surface), the geometric optics (GO) Kirchhoff approximation applies, whereas the small perturbation model (SPM) is adequate when the wavelength is large compared to the RMS height (Ishimaru, 1997). A small example in Fig. 2 shows that the sign of the phase dependence of these models is opposite to the dielectric model by Hallikainen et al. (1985) and indeterminate for the one by Peplinski et al. (1995); the magnitude, however, is much smaller for the surface models. This small dependence of φ has often been considered negligible compared to the noise level or other influences (De Zan et al., 2014; Rudant et al., 1996).

4. Data sets

The airborne L-band data acquired during two campaigns are considered in this study. The first one is the Agrisar 2006 campaign in north-eastern Germany, the second one is the Canadian Experiment for Soil Moisture 2010. In both cases in-situ soil moisture measurements are available. The campaigns differ with respect to the temporal intervals of the acquisitions and the vegetation cover. Neither was designed for the analysis of soil moisture effects on interferometry, and this is particularly evident with respect to vegetation dynamics and additional sources of decorrelation such as ploughing.

4.1. Agrisar 2006

The objective of this campaign was to provide data for an improved understanding of remote sensing measurements over agricultural vegetation. The study site is located around Görmin, Mecklenburg–Western Pomerania, Germany (53° 58′N 13° 16′E). The temporal extent effectively covers one growing season for the crops present (German Aerospace Center, 2008): winter wheat, maize, rape, sugar beet, and barley; several small towns and patches of mixed forest are also included (see Fig. 3). The topography is flat, with a slight slope towards a nearby river and several drainage features perpendicular to the latter (Zwieback & Hajnsek, 2014). The soil is dominated by sandy loam and similar textures, with clay contents of less than 10% (German Aerospace Center, 2008).

The airborne L-band ($\lambda = 0.23$ m) SAR data were acquired by the E-SAR system in intervals of one to two weeks at a range (azimuth) resolution of about 2 (1) metres (German Aerospace Center, 2008). The subset of images used in this study were recorded from the same track at a
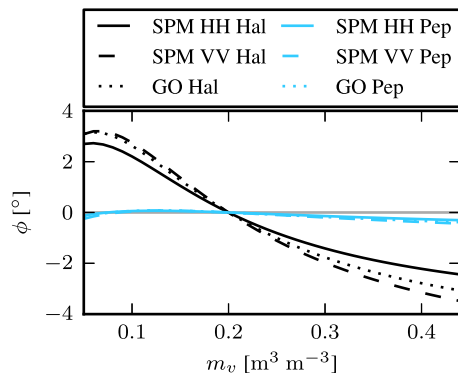
Fig. 2. Predictions for the interferometric phase due to surface scattering as a function of slave m_v for a master soil moisture of 0.2 m³ m⁻³. GO is the polarization-independent Geometric Optics approximation, SPM the Small Perturbation Model. Hal is the mixing model by Hallikainen et al. (1985), Pep the one by Peplinski et al. (1995).

Fig. 4. Double difference phase ϕ and coherence |γ| of Agrisar ROI 230× are shown in the top panel; the common master acquisition at DOY 163. The changes in soil moisture m_v and biomass b with respect to this master scene are given in the lower panel.

nominal baseline of 0 m. They were acquired around noon local time on the dates shown in Fig. 4. The interferometric phase and coherence with respect to the image taken at DOY 163 of a wheat field are shown in the first panel.

Two corner reflectors provide a reliable phase reference in their vicinity. As shown in Fig. 3, there are considerable large-scale phase trends present in the data. The interferometric phase has clear correspondences with certain field boundaries, which correspond to differential deformation estimates between the fields. The impact of the additional phase patterns is minimized by using stable scatterers in addition to the corner reflectors, cf. Section 5.1.3.

Several soil- and plant-related parameters were measured contemporaneously with the airborne acquisitions: the ones used in this investigation are soil moisture, vegetation height and wet biomass. The volumetric soil moisture m_v [m³m⁻³] was measured manually at three locations (by Time Domain Reflectometers (TDR); 0–5 cm depth) within each field within 1 to 2 h of the radar acquisitions. These measurements were subsequently averaged. The sampling of the measurements of the wet biomass b [kg m⁻²] and vegetation height h [cm] was conducted analogously, the former being determined by clearing 1 m² and weighing. The fields for which such data are available are compiled in Table S1. The temporal evolution of these parameters is shown for one of the fields in Fig. 4. The soil moisture tends to decrease over time until June 13, when it reaches $m_v = 0.12$ m³ m⁻³. Subsequently, there is a rain event followed by a dry-down period. The biomass b of the wheat field increases monotonically until June 21, when it reaches a value of 5.6 kg m⁻², before it declines as the plants reach the period of senescence.

4.2. CanEx2010

The aim of the Canadian Experiment for Soil Moisture in 2010 (Magagi et al., 2013) was to support calibration, validation and algorithm development activities for the SMOS and SMAP satellite missions; to this end, in-situ measurements of soil and vegetation properties were taken from June 2–14 2010. Among the remote sensing data gathered are six UAVSAR acquisitions over the Kenaston, Saskatchewan, Canada, test site (51° 30′ N, 106° 18′ W). This flat area is characterized by predominantly rainfed agricultural fields, pastures and grassland and at least 1.5% of open water surfaces. Before the campaign wet weather conditions had prevailed, leading to an increase in the extent of standing water. The fields had been tilled and were covered by a varying amount of residue (Magagi et al., 2013).

The quadpol UAVSAR data (L-band: $\lambda = 0.24$ m) have a resolution of 1.7 m (0.8 m) in range (azimuth) (Jones & Davis, 2011). They were acquired in irregular intervals between one and three days with a nominal baseline of 0 m at 3 pm local time. The lack of corner reflectors implies that the unknown phase offsets in the data have to be eliminated by e.g. forming differences with stable scatterers. The phase patterns are more stable than in the Agrisar campaign, which can be seen in the interferogram of Fig. 5.

Volumetric soil moisture m_v was measured hourly at permanent stations by Environment Canada (EC) using Stevens Hydraprobe probes in several depths, of which the 0–5 cm vertical sensor (using an improved factory calibration) will be considered. In addition, visual assessments of the tillage, vegetation cover and crop type are available for most fields (Magagi et al., 2013). The fields for which such measurements are available at all acquisitions are compiled in Table S2. The locations of these
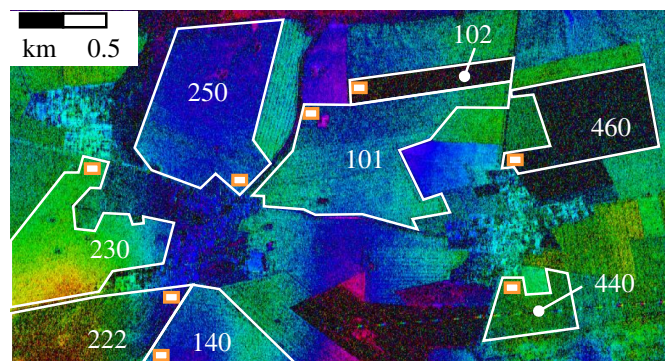

Fig. 3. Agrisar interferogram between acquisition of DOY 163 and 185: the unreferenced phase is given by hue (full colour circle), the coherence magnitude by the intensity. Certain phase patterns correspond to field boundaries (white lines), others relate to spurious trends, especially in near range (bottom of image). The regions of interest of each field are given by the white and orange rectangles, the field number is annotated in white.
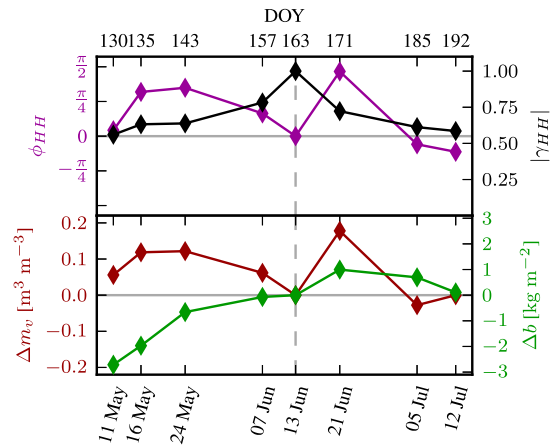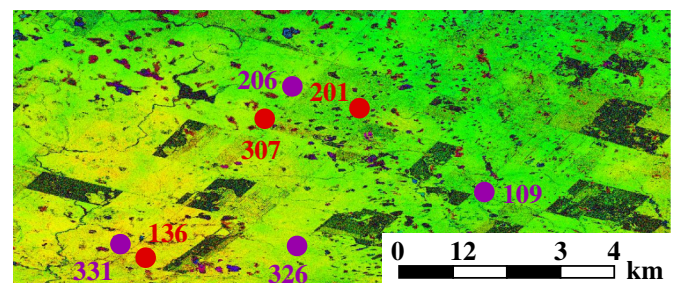

Fig. 5. Interferogram between DOY 156 and 165 of the CanEx2010 campaign. As in Fig. 3 the near-range region is at the bottom of the image and also the colour codes correspond. The location of the soil moisture probes is given by the red and purple dots, which are annotated with the code of the field.

measurements are shown in Fig. 5 and annotated by the number of the field. Note that the dynamic range in the measured soil moisture, i.e. the difference between the maximum and minimum value, varies by about a factor of 10 between the different fields. This might be related to e.g. variations in soil texture and other soil properties, as well as the microtopography.

The temporal pattern of the soil moisture evolution is, by contrast, very stable across the different probes. One example is given in Fig. 6, where the changes with respect to the master acquisition at DOY 165 ($m_v = 0.23$ m^3 m^{-3}) are given. They show a close correspondence to the precipitation measured at field 136, which led to a wetting in the middle of the campaign.

5. Data analysis

5.1. SAR processing

5.1.1. Interferogram formation

The complex interferograms were formed for all possible pairs, which results in a total of 28 interferograms in the Agrisar campaign, and 15 in the CanEx2010 experiment. The number can depend on the field (due to harvesting or ploughing) and can be found in Tables S1 and S2. A flat earth and topographic phase correction, along with range spectral filtering, was applied (Bamler & Hartl, 1998). The Agrisar data showed larger deviations from the intended zero $B_\perp$ condition, with the height sensitivity $|\kappa_z|$ generally bounded by 0.05 m^{-1}: a difference in the elevation model error at two points of 2 m would thus correspond to a phase error of 0.1 rad, which is considerably smaller than the dynamic range observed in the data. Larger height errors are only expected for phase references on top of isolated man-made structures such as buildings.

5.1.2. ROI definition

Within each field a region of interest (ROI) in the shape of a rectangle (50 m in range, 100 m in azimuth) was chosen in such a way that the target was as homogeneous as possible. For the Agrisar campaign, the choice of location of the ROI was dictated by the presence of the spurious phase patterns. The ROI was taken to be as close to a persistent scatterer as described in Section 5.1.3 as possible. In the CanEx2010 data set, the ROI was taken to be as close to the soil moisture probe as possible. Difficulties and heterogeneities of the observed phases are mainly related to the presence of water surfaces that are partially covered with vegetation. In either campaign and at each of the four corners of this rectangle, 172 looks L were averaged to obtain the coherence information, corresponding to a rectangular box car filter. These subROIs are coded by
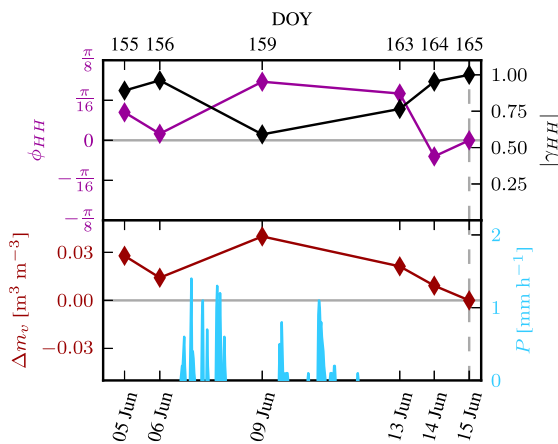

Fig. 6. Interferometric phase ϕ and coherence magnitude $|\gamma|$ at HH for ROI 326b of the CanEx2010 experiment. These are taken with respect to the common master at DOY 165. The lower panel shows the changes in soil moisture with respect to this master acquisition as measured in this field. The blue bars denote the precipitation rate measured in field 136.

their field number (three digits) followed by a letter: v–y for Agrisar, a–d for CanEx.

5.1.3. Phase reference

The unknown phase offset in each interferogram and for each ROI can be removed by forming differences with respect to stable scatterers. In the absence of corner reflectors, one commonly resorts to a data-driven approach (Ferretti et al., 2011). We do so by finding persistent scatterers (PS) using the amplitude-based signal-to-clutter ratio method (Kampes, 2006). As the amplitude criterion is not sufficient for a pixel to be stable, the three closest ones are taken for each ROI, and among these two are chosen. The first, the nearest one, is based on the rationale that phase errors due to e.g. inaccuracies in the flight track increase with distance. The second – the one among the three with the smallest phase variance – will potentially rule out unstable targets, as these are characterized by larger fluctuations. The impact of this decision rule is studied empirically in Section 6.4.

For a given ROI and its persistent scatterer, the difference between the phase over the field and over the PS is formed. This so-called double difference (Kampes, 2006) will be referred to as simply the phase ϕ of the ROI. This implicitly assumes that the phase of the PS is stable. The deformation associated with this phase ϕ thus corresponds to an apparent movement of the ROI with respect to the persistent scatterer. This phase did not have to be unwrapped as no phase wrapping was observed in the data. The double-difference phase is still affected by phase patterns associated with orbital errors and tropospheric influences. Their impact is expected to be mainly determined by the spatial separation of the PS and the ROI (Hanssen, 2001). These distances are given for each field in Tables S1 and S2.

In the Agrisar campaign, the spurious phase patterns have a typical wavelength of more than 2.5 km (see e.g. Fig. 3). For an average spatial distance to the PS of 100 m, this corresponds to a phase error of 14°, which is not expected to be correlated with soil moisture changes. In the CanEx2010 data, the typical separation of 300 m corresponds to a phase error 5° given a spatial scale of the phase patterns of 20 km. The tropospheric influence is partially included in these numbers, and is expected to be smaller (<2°) (Emardson, Simons, & Webb, 2003; Goldstein, 1995).

5.2. Regressions

The connection between the observables and explanatory parameters (such as m_v) is studied by regressions, whereby it is assumed that the observable can be described by simple functions of said parameters. In the Agrisar campaign, during which sizeable vegetation growth and senescence occur, the vegetation is described by the wet biomass b. This parameter is expected to be closely related to the backscattered power and the optical path through the canopy (Ulaby, Tavakoli, & Senior, 1987). As the vegetation height was also measured, it will be included in separate regression to study the robustness with respect to the characterization of the vegetation. In general, these vegetation parameters are denoted by v. For the CanEx campaign, the fields were bare or covered by harvest residues, so that no vegetation terms are included in the model.

5.2.1. Regression model

For the coherence $|\gamma| \in [0, 1]$, which is invariant to the choice of master/slave, the following structure is postulated:

$$log\left(\left|\gamma_{ij}\right|\right) = \beta_0 + \beta_{m_v}|\Delta m_v| + \beta_t|\Delta t| + \beta_v|\Delta v| + \varepsilon_{ij} \qquad (2)$$

i.e. the terms are assumed to affect $|\gamma|$ in a multiplicative fashion, thus rendering negative coherences impossible. The coefficient β_{m_v} represents the decorrelation due to $|\Delta m_v|$, whereas β_v denotes the impact changes in the vegetation parameter that Δv has on the coherence magnitude. The temporal decorrelation is assumed to be related to the time

separation between the two acquisitions Δt; it is quantified by the coefficient β_t. The error term of the i, j interferogram is denoted by ϵ_{ij} (with expected value of zero), and t is the temporal separation.

The phase ϕ is assumed to be governed by

$$\phi_{ij} = \beta_{m_v} \Delta m_v + \beta_v \Delta v + \epsilon_{ij} \tag{3}$$

where the absence of an intercept term is due to the expectation that no change in the exogenous variables corresponds to zero ϕ.

The structure of the phase triplets is complicated, as they i) depend on three acquisitions, and ii) deviate from zero only in the presence of decorrelation. They are thus analysed separately in Section 5.3.

5.2.2. Stochastic model

The phase noise ϵ_{ij} is often considered to be due to two kinds of components (Kampes, 2006): the first ε_{ij}, due to the correlation properties of the particular interferogram, can e.g. be described within the Gaussian speckle model (Bamler & Hartl, 1998); the second ξ_i, due to a phase offset of each SLC image i from e.g. the atmosphere, is here assumed to be stationary in time. Thus $\epsilon_{ij} = \varepsilon_{ij} + \xi_i - \xi_j$, with ε and ξ assumed uncorrelated. The second moments of ϵ_{ij} then evaluate to

$$\begin{aligned} \langle \epsilon_{ij}\epsilon_{kl} \rangle &= \langle \varepsilon_{ij}\varepsilon_{kl} \rangle + \langle \xi_i \xi_k \rangle + \langle \xi_j \xi_l \rangle - \langle \xi_j \xi_k \rangle - \langle \xi_i \xi_l \rangle \\ &= \sigma_{ij}^2 \delta(ij, kl) + \Sigma^2 [\delta(i,k) + \delta(j,l) - \delta(j,k) - \delta(i,l)] \end{aligned} \tag{4}$$

where $\delta(u, v)$ is a Kronecker delta and the correspondence between the two equations is term by term. The value of σ_{ij}^2 is estimated from the observed γ_{ij} based on the Gaussian speckle model Cramer–Rao bound, relative to σ_0^2, which is the value for the given number of looks L that would be obtained for $|\gamma| = 0.5|$. The ratio $\kappa = \Sigma^2/\sigma_0^2$ is estimated in the regression model from the data. A simplified analysis without autocorrelations is also conducted to study the robustness with respect to the stochastic model.

5.2.3. Implementation

The regressions for $|\gamma|$ are obtained by ordinary least squares, the ones for ϕ by Maximum Likelihood estimation assuming Gaussian noise using the nlme package in R (Pinheiro & Bates, 2000; Pinheiro, Bates, DebRoy, Sarkar, & R Core Team, 2013). Standard regression diagnostics (Judge, Hill, Griffiths, Lutkepohl, & Lee, 1983) are used to remove outliers (Bonferroni-corrected t-test of studentized residuals with $\alpha = 0.05$). In addition to the point estimates of β, the decisions of the Shapiro–Wilk test for normality at $\alpha = 0.05$, and the 95% confidence intervals for β are reported. Note that the latter are i) based on the normality hypothesis, and ii) are only approximate if κ is estimated.

5.3. Quantile regressions of Ξ

In contrast to all other hypotheses, the dielectric volume model predicts non-zero phase triplets. As the sign of these phase triplets depends on the ordering of the acquisitions, we propose to focus on their magnitude $|\Xi_{ijk}|$ and parameterize it as a function of max $|\Delta m_v| > 0$, i.e. the maximum of all three $|\Delta m_v|$:

$$|\Xi_{ijk}| = \beta_0 + \beta_{m_v} \max|\Delta m_v| + \beta_v \max|\Delta v| \tag{5}$$

where the vegetation change term v is only included for the Agrisar campaign. The regressand $|\Xi_{ijk}|$ is non-negative: its spread and thus its median is expected to increase with max $|\Delta m_v|$ in the dielectric framework, but in a complicated fashion as it depends on all three values of m_v and the particular parameterization and model. In order to study this behaviour in a robust way, median regression is employed to estimate the coefficients β. The standard errors are computed according to the rank-inversion method (Koenker, 2005, 2013).

6. Results

6.1. Exploratory data analysis

The impact of m_v on the different observables is exemplified in several scatter plots in Fig. 7; these were chosen to be representative of the different kinds of relations found in the data. The phase values (Fig. 7a)–h)) predominantly show a positive, approximately linear trend with Δm_v. The correlation, however, differs: in field 230x, for instance, the scatter around the fitted curve is smaller in HH than in VV, where it seems to increase with the temporal separation Δt. Differences are also conspicuous with regards to the magnitude of the effect, e.g. field 307a.

The magnitudes of the coherence $|\gamma|$ in subfigures i) and k) both decrease with $|\Delta m_v|$, with the apparent influence of Δt being more pronounced for 230x. The influence of this temporal decorrelation is also evident in Fig. 4, where both biomass and soil moisture return on DOY 192 to the values observed during the master scene. However, the coherence magnitude does not return to values close to one. By contrast, such a return can be observed in Fig. 6, where both soil moisture and coherence show similar temporal behaviour.

Also the phase triplets $|\Xi|$ exhibit such diversity: the ones in field 230x (subfigure j)) are an order of magnitude larger on average than the ones of 136a (l)), with neither displaying a conspicuous dependence on the maximum soil moisture.

6.2. Regression results

6.2.1. Agrisar campaign

The estimated soil moisture regression coefficients β of both phase and correlation are plotted in Fig. 8 for the Agrisar campaign. For log $|\gamma|$ in HH, all but a single one are negative. The deviation, however, is not necessarily significantly different from zero ($\alpha = 0.05$): such significant effects are found for 50% of the samples in HH, 21% in HV, and 36% in VV. However, between these polarizations, the differences of the size of the effect for any particular field are generally (>90%) smaller than the uncertainty, cf. Table S3 for a list of the differences.

The impact of soil moisture variations on the phase ϕ is found to be significant for 71% of the samples in HH, 39% in HV, and 43% in VV. All the estimated effects of these significant samples are positive. The size of the effect $\beta_{\Delta m_v}$ exceeds 2 rad m^{-3} m^3 (this corresponds to a phase change of 23° for $\Delta m_v = 0.2$ m^3 m^{-3}) in 82% of the samples in HH, 53% in HV and 46% in VV.

Not only the soil moisture m_v but also the biomass b is seen to impact the observables: the estimated regression coefficients are shown in Fig. 9. The effects on $|\gamma|$ are predominantly negative (a notable exception being 101v), and significantly different from zero for about 35%–55% of the samples. An increase in biomass is seen to affect ϕ in the same direction as an increase in m_v: all significant effects $\beta_{\Delta b}$ but two are positive. This significance is found for 32% of the samples in HH, 61% in HV, and 82% in VV. The impact over all the crops except sugar beet is less than 1 rad kg^{-1} m^2, and more pronounced in VV than in HH over wheat (230, 250) and barley (440), cf. Table S4.

6.2.2. CanEx campaign

The analysis of the CanEx data, where the vegetation is not subject to significant changes, also reveals a positive dependence of ϕ on m_v, albeit with different magnitudes. These are also exceedingly variable, with e.g. field 201 showing a 10 times larger impact than field 109; the magnitude of the latter (2–4 rad m^{-3} m^3) being comparable to the one found in the Agrisar data set. The fields with the highest coefficients $\beta_{\Delta m_v} > 10$ rad m^{-3} m^3 are those in which the soil moisture measurements exhibit small variations <0.1 m^3 m^{-3}, see Table A2.

These effects $\beta_{\Delta m_v}$ are significant at $\alpha = 0.05$ for 86% in HH and HV, and 82% in VV; between these polarizations, the difference in magnitude is generally smaller than the uncertainty, see Table S4. Exceptions
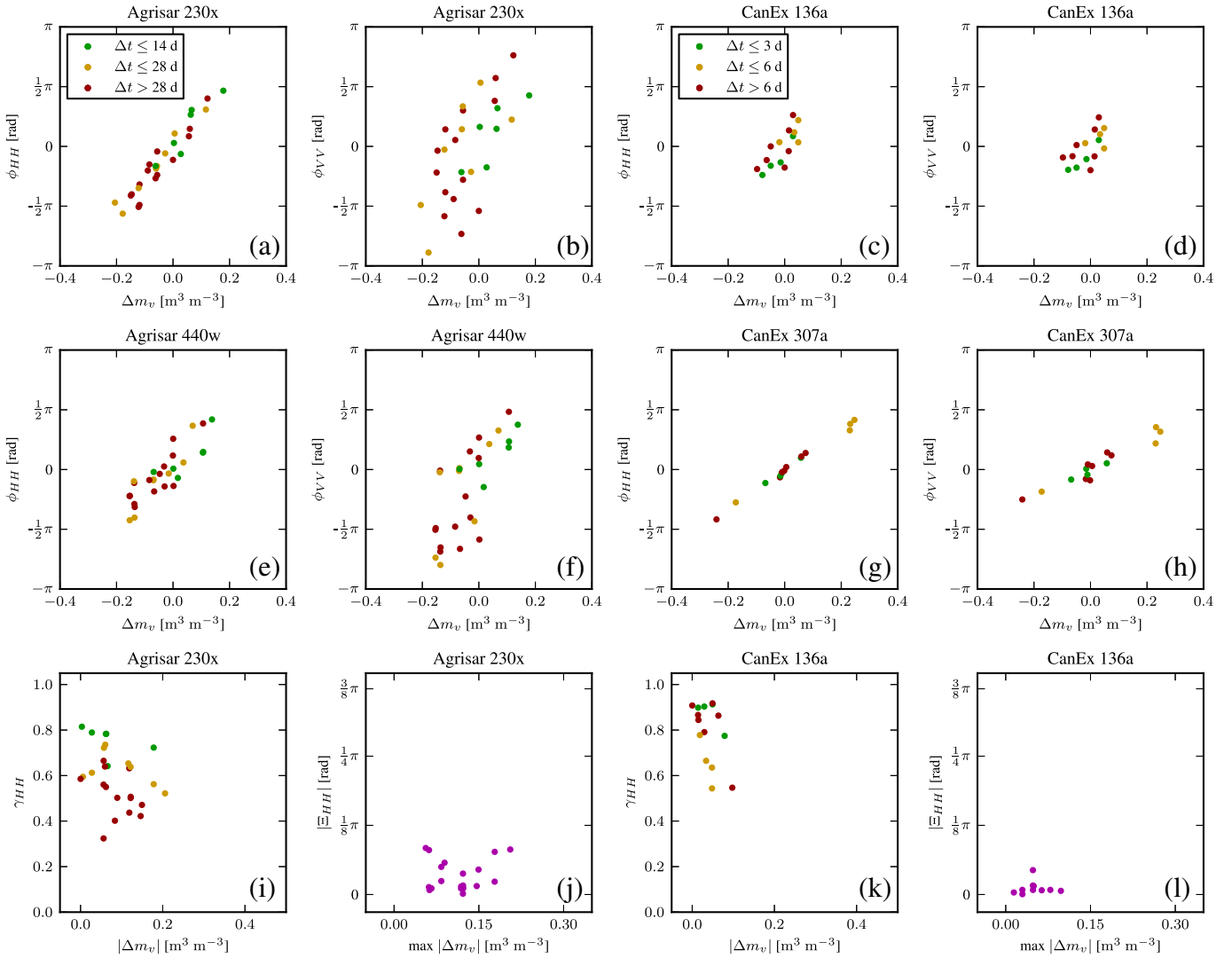
Fig. 7. Scatter plots of the observables (or function thereof) versus m_v. The colour for γ and ϕ encodes the temporal difference Δt in days and differs for Agrisar/CanEx.

include field 307, where also the variation of the effect observed in different parts of the field exceeds the uncertainty. The estimated soil moisture impact on the coherence magnitude is found to be significant for around 57% of the samples in all polarizations. Negative coefficients prevail in all polarizations, with field 201 being a notable exception.

6.3. Quantile regression

The median of $|\Xi|$ turns out not to depend significantly on max $|\Delta m_v|$ in the Agrisar campaign (Fig. 11). The significant deviations from zero are in line with what would be expected based on random variations under the null hypothesis. This also applies to most fields in the CanEx campaign (Fig. 12): ROIs 307 and 326 form an exception, the former in particular in HV, the latter in HH.

6.4. Sensitivity analysis

The previous analysis is based on several algorithmic choices introduced in Section 5. As the main trends and patterns turn out not to be severely affected, the relevant figures and tables are attached as

supplementary materials. The impact of each of the identified choices will be briefly sketched in the following.

6.4.1. Reference phase

The phase observable ϕ is sensitive to the reference phase with respect to which it is determined. The second implementation of its retrieval, which is based on the identified persistent scatterer for which the smallest phase variance is obtained, yields the phase sensitivities shown in Fig. S1 for the Agrisar campaign and for the CanEx data set in Fig. S2. For the former the sensitivities decrease for fields 230 and 440 (partially ceasing to be significant), whereas the opposite trend is observed over field 460. A similar decrease in the effect occurs for fields 109 and 201 in the CanEx campaign, whereas fields 326 and 331 cease to display any sensitivity to m_v.

6.4.2. Vegetation parameterization

The amount of vegetation as well as changes therein can also be parameterized by the vegetation height h instead of the wet biomass b in the Agrisar campaign. The soil moisture sensitivities of ϕ and $log(|\gamma|)$ are plotted in Fig. S3: neither those of the coherence nor those of the phase change by more than one standard error. In the vast majority of cases
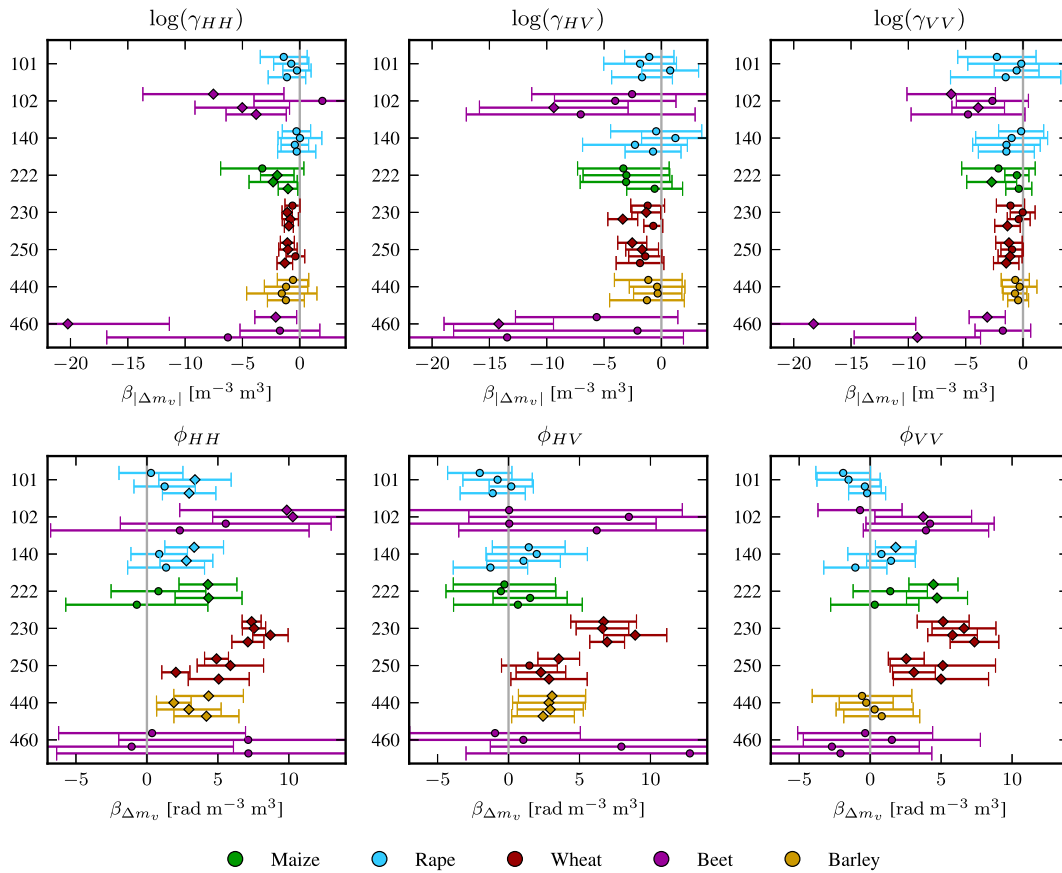
Fig. 8. The soil moisture coefficients of the regression models for the magnitude (top row) and phase (bottom row) of the complex coherence grouped according to the fields in the AGRISAR campaign: for each field there are four subROIs v–y. The error bars indicate the 95% confidence intervals; diamonds a significant deviation from 0.

the differences are much smaller than that; exceptions are the phase sensitivities of the rape fields, for which the model based on h yields significant Δm_v terms in HH and HV. The results of the median regression on $|\Xi|$ are virtually unaffected, see Fig. S4.

6.4.3. Autocorrelation

The regressions on ϕ rely on the stochastic model of Eq. (4): it represents correlations between the observations, and these are parameterized by κ. The results of the simplified stochastic model for which this parameter is set to 0 are shown in Figs. S5 and S6. The former shows that for the Agrisar campaign the $\beta_{\Delta m_v}$ coefficients remain predominantly positive and of similar magnitude; differences include the appearance of a significant negative instance (101 in HV and VV) or significant positive ones (e.g. 440 in VV) and the loss of significance for the field 250 in VV. In the CanEx data set, no similar changes occur.

6.4.4. Normality

The confidence intervals of the regressions of ϕ and log $|\gamma|$ rely on the assumption of normality for the error term ϵ_{ij} in e.g. Eq. (2). The results of the relevant hypothesis test (see Section 5.2) are summarized in Table A5. The null hypothesis is discarded for around 15% of the subROIs at $\alpha = 0.05$, which in the Agrisar campaign corresponds to about 5 instances. In most cases the numbers of rejections are more than what would be expected if the error terms were normally distributed in all subROIs and independent of each other. A closer inspection of the results, however, shows that the deviations from normality tend to be clustered according to the fields, thus rendering the assumption of independence inherent in the binomial test invalid. Irrespective of this violation, the total number of instances with significant deviations from normality is rather small, e.g. 1–7 for the ϕ models in either campaign.

7. Discussion

7.1. Impact on observables

7.1.1. Phase

The positive phase coefficients $\beta_{\Delta m_v}$ – they tend to prevail in both campaigns and all polarizations – are only consistent with the dielectric hypothesis of Table 1, but not with the penetration depth or deformation explanation. The magnitude, although highly variable, generally exceeds the sensitivities obtained from the surface-only models in Fig. 2 by about two orders of magnitude. Instead, it is more congruous with a volume contribution. The scatter in magnitude could be partially explained by the difficulty of calibrating m_v and soil permittivity measurements, their spatial scale and the depth dependence. The connection between the size of the phase coefficients $\beta_{\Delta m_v}$ and the dynamic range of the measured soil moisture is indicative of such a problem affecting the soil moisture measurements. It could also reflect differences in physical properties that affect both the scattering and the hydrological behaviour of the soil. These might be related to soil texture or surface roughness. A non-linear dependence of the phase on soil moisture could also result in such an apparent relation between the soil moisture dynamic range and the interferometric phases.

The phase coefficients of the biomass term $\beta_{\Delta b}$ in the Agrisar campaign tend to be positive as well; and all the significant ones ($\alpha = 0.05$) are. This sign is also consistent with a dielectric mechanism: an increase in biomass (assumed closely related to total water content) above affects the optical path of the wave in a similar way that an increase in m_v does in the soil dielectric model. This influence was observed previously for vegetation at X-band in laboratory experiments by (Rudant et al., 1996).
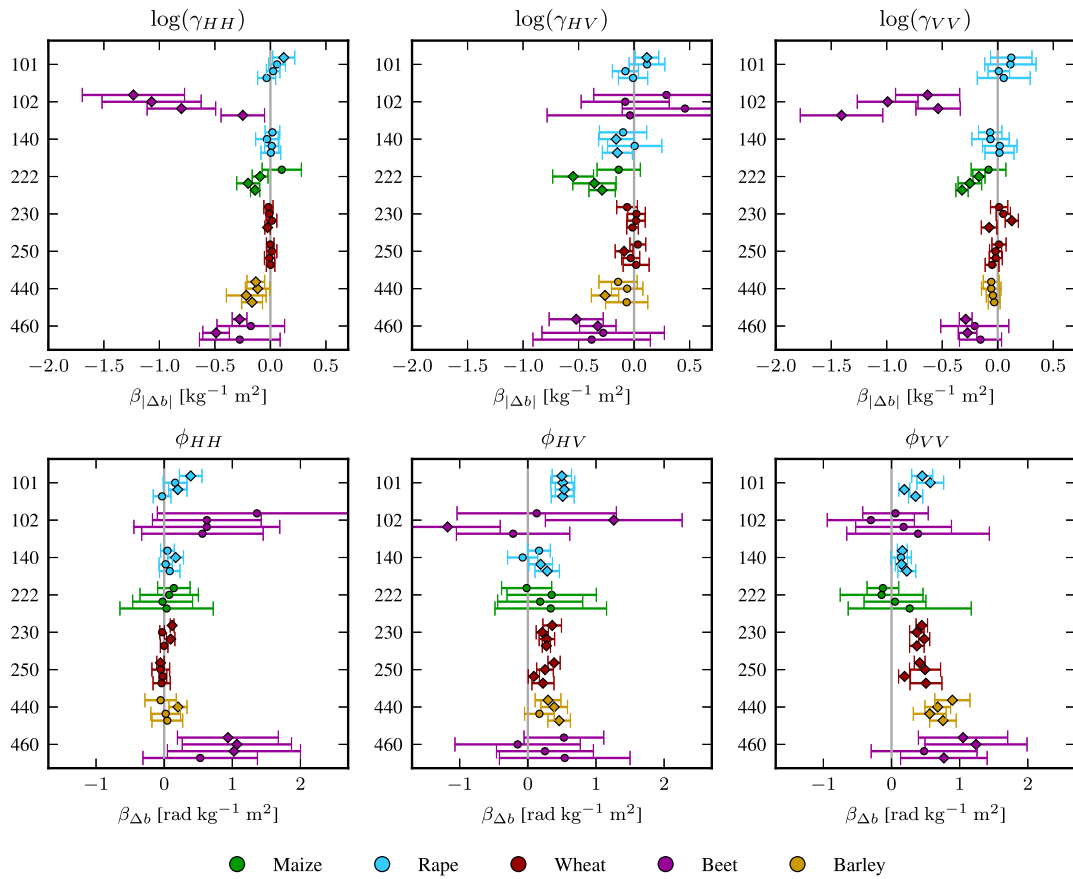
Fig. 9. The biomass coefficients of the regression models for the magnitude (top row) and phase (bottom row) of the complex coherence, cf. Fig. 8 for a description.

The positive sign of the soil moisture dependence inferred from the regression analysis was also found by Rudant et al. (1996) in the previously mentioned study: for a sandy soil the authors partitioned this phase change into a compaction (due to the particular kind of application of the water; measured independently) and a complementary effect, both of which had the same sign. They did likewise for a swelling soil and concluded that the complementary effect had the same sign as for the sandy soil, but could not provide a more quantitative analysis due to lack of near surface soil moisture measurements. Similar measurements between 1.5 and 10 GHz showed the same sign of the phase change. The interpretation of these results is hampered by i) lack of displacement measurements, and ii) the sizeable deviations from uniform soil water profiles (Nesti et al., 1998; Rudant et al., 1996). In a different experiment, Morrison et al. (2013) found only negligible phase changes upon wetting of a homogeneous sand sample (C-band laboratory experiment; deformations monitored by monoscopic photogrammetry). Application of the same measurement constellation to a different homogeneous sand sample found the opposite phase trend (Morrison et al., 2011), i.e. in line with the penetration depth hypothesis or surface scattering. The sensitivity of the phase to Δm_v was observed to vary by about one order of magnitude over the homogeneous soil sample. These phases could not be explained by deformations. They are similar in size and sign to the ones observed in a laboratory experiment by Yin et al. (2014) in S-band, who concluded that the SPM surface scattering model could explain the observed phases.

Based on L- and C-band satellite data over three fields in Ireland, Barrett et al. (2013) found linear dependencies of ϕ on Δm_v of both signs. In the majority of cases, these linear dependencies were, however, not significant. Over a swelling soil, te Brake et al. (2013) also found a negative dependence of ϕ on Δm_v but concluded that it was consistent with the observed deformations.

7.1.2. Coherence

The majority of estimated $|\Delta m_v|$ coefficients for the coherence $|\gamma|$ are negative: this means that changes in soil moisture are associated with a loss of correlation. Such decorrelation is consistent with the volume dielectric hypothesis, but not with a pure surface contribution. The penetration depth explanation does not allow a prediction of this trend, whereas the latter depends on the detailed modelling assumptions for the deformation hypothesis. Note that this dependence was found to be significant at $\alpha = 0.05$ for less than one half of the samples. This low percentage is particularly pronounced for the Agrisar campaign at all polarizations considered, and could be due to

1. The larger time gap between acquisitions;
2. m_v and b are correlated with each other and with time: this multicollinearity inflates the standard errors of $\beta_{|\Delta m_v|}$;
3. Pronounced vegetation growth dominating decorrelation;
4. Additional temporal decorrelation due to wind-induced movements and dielectric changes within the plant.

The latter are difficult to quantify, especially given the large structural changes due to plant growth and the lack of suitable wind speed measurements. The impact of wind-induced decorrelation on vegetated areas is well known (Zebker & Villasenor, 1992), in particular for forests (Lavalle, Simard, & Hensley, 2012). In a tropical rain forest, Hamadi, Albinet et al. (2014) and Hamadi, Borderies et al. (2014) observed that wind-related movements, structural changes of the canopy and permittivity fluctuations of plant tissue led to decorrelation at different time scales. The influence of vegetation dynamics on decorrelation was also observed by Barrett et al. (2012) in agricultural fields in Ireland at both C and L-bands: the effect of soil moisture changes was small in comparison. Srivastava and Jayaraman (2001) and Weydahl (2001)
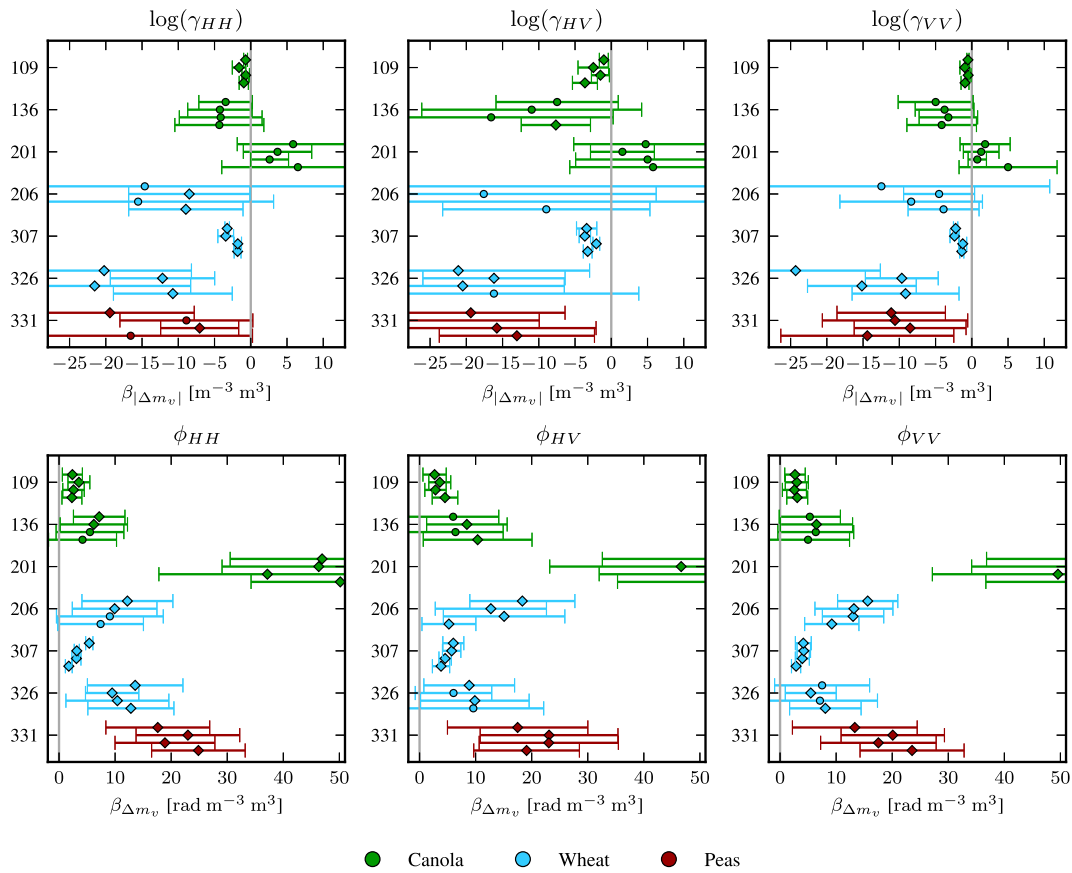
Fig. 10. The soil moisture coefficients of the regression models of the CanEx campaign, cf. Fig. 8 for a description.

deduced that decorrelation was related to changes in plant and soil moisture, but did not provide quantitative results due to lack of soil moisture observations. The decorrelation observed in this study is also consistent with the results of Hensley et al. (2011). Using the CanEx data set but different ROI definitions and statistical techniques, they deduced that the time lag alone cannot explain the decorrelation but that soil moisture information is needed. Furthermore, the magnitude of these decorrelation effects is similar to the ones obtained by Nesti et al. (1998) in a laboratory experiment at higher frequencies.

7.1.3. Phase triplets

The results in Figs. 11 and 12 reveal that the median of $|\Xi|$ has an insignificance linear dependence on max $|\Delta m_v|$ except for two fields in the CanEx campaign: this is consistent with the deformation, null,

penetration depth and surface-based dielectric hypothesis, but not necessarily with the volume dielectric explanation. The origins of this insignificant dependence appear to be distinct for different fields. Firstly, there are fields for which the linear model for ϕ can describe the data exceedingly accurately: in this case the Ξ are close to 0 and the fit for the median of $|\Xi|$ is good and close to 0 as well. Among these fields are CanEx 109, as well as Agrisar 230 and 250. The second category includes those fields whose fit to both ϕ and $|\Xi|$ is inaccurate, such as Agrisar 102 and 460, as well as CanEx 331. Note that this cannot be due to phase offsets alone (such as those arising from the phase referencing) as these cancel when the phase triplets are formed. Thirdly, there are fields for which the linear model for ϕ applies reasonably well, but for which the $|\Xi|$ (which indicate deviations from linearity) are not clearly dependent on max $|\Delta m_v|$, e.g. CanEx 136 (see Fig. 7) or Agrisar 140.
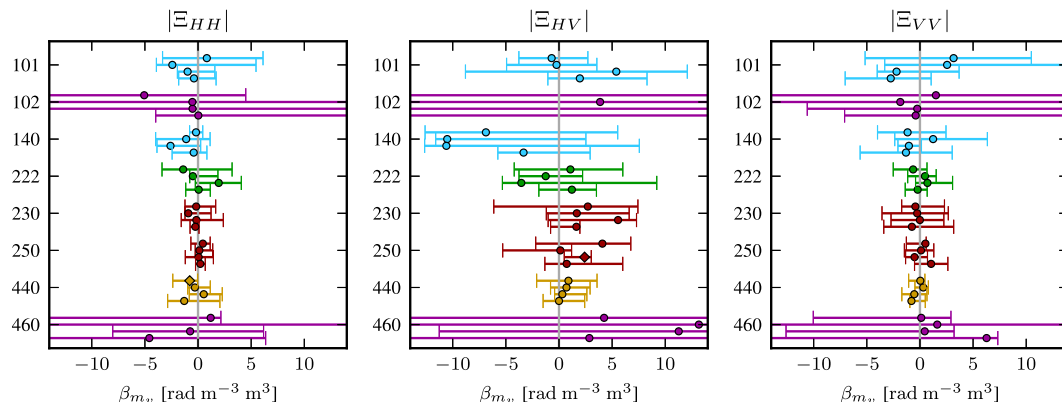

Fig. 11. The soil moisture coefficients of the Ξ quantile regression model of the AGRISAR campaign, cf. Fig. 8 for a description.
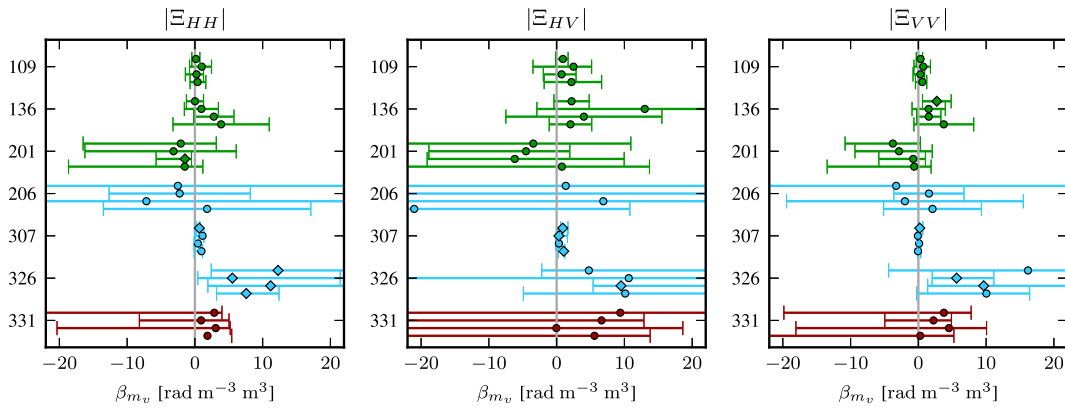
Fig. 12. The soil moisture coefficients of the Ξ quantile regression model of the CanEx campaign, cf. Fig. 8 for a description.

De Zan et al. (2014) compared the phase triplets with the predictions of the volume-only first-order scattering model for field 222 in the Agrisar data set, for which they found a clear correspondence. The model-independent results of Fig. 11 do not confirm a dependence on soil moisture, but neither do they rule out different functional forms of dependence, i.e. the assumed dependence of Eq. (5) might be incapable of capturing the soil moisture effects (see Section 5.3). This suggests the need for more detailed assessments of such physical models.

7.2. Assessment of explanations

The previous analyses of the observed relation between the DInSAR observables and soil moisture permit certain inferences about the plausibility of the four proposed hypotheses of Section 3.

7.2.1. Null hypothesis

The null hypothesis – there is no impact on any observable – cannot explain the significant and non-zero dependences observed for ϕ and $|\gamma|$. These inferred connections can, of course, be spurious, e.g. due to omitted variables or only partially considered phenomena that influence the observables. These include the phase influences due to DEM errors and orbit inaccuracies. However, these are not expected to be correlated with soil moisture changes, and estimated to be smaller than the inferred soil moisture contributions on the phase. Another prominent example of such a phenomenon is vegetation, which exerts a considerable influence in the Agrisar campaign. In the CanEx data set, however, the limited vegetation cover and growth, along with the short repeat periods, provide more support for the actual presence of soil moisture effects. Secondly, the soil temperature T_s has been repeatedly shown to impact the soil dielectric constant (Mironov et al., 2013); however, T_s only varies by about 4 K for the different acquisitions in the CanEx campaign, which translates to changes in permittivity that are much smaller than the ones due to soil moisture (in the model by Mironov et al. (2013), it is equivalent to $\Delta m_v \approx 0.001$ m^3 m^{-3}). The results of Figs. 8 and 10 thus provide evidence for the presence of soil moisture effects.

7.2.2. Deformation

The deformation hypothesis (soil swelling) predicts a different sign of $\beta_{\Delta m_v}$ for ϕ than the one observed in both data sets. It can thus be ruled out as the sole origin of an m_v influence of the phase. The opposite deformation behaviour (swelling upon drying) would be consistent with the sign of $\beta_{\Delta m_v}$; we have, however, found no reference to such a soil in the literature, except for rain compaction (Moore & Singer, 1990). The latter is, however, too small a deformation to explain the measured ϕ: it can reach almost π (no apparent wrapping has been

observed): this corresponds to a deformation of $\frac{\lambda}{4}$, i.e. 0.05 m, and this appears to be a peculiarly large displacement (Hensley et al., 2011).

7.2.3. Penetration depth

The penetration depth mechanism also predicts the opposite sign for the phase dependence than the one present in the data. In conjunction with the inherent inadequacies of this hypothesis (in particular the inability to explain $|\gamma|$), these empirical results contradict the penetration depth explanation.

7.2.4. Dielectric mechanism

The dielectric volume explanation can account for the observed dependencies of both ϕ and $|\gamma|$ (bearing in mind the difficulties with the latter identified in Section 7.1.2). The magnitudes of the phase effects are furthermore inconsistent with a pure surface dielectric effect as predicted by the surface scattering models considered in Table 2. The volume-only model of De Zan et al. (2014) predicts not only the sign but also the right order of magnitude for $\beta_{\Delta m_v}$ of ϕ. This model also predicts non-zero phase triplets Ξ. Their dependence on soil moisture as expressed by Eq. (5) is found insignificant for the majority of the fields, but the functional relation predicted by the model by De Zan et al. (2014) is different as well as more complex than the one assumed in the regression. The absence of significance found in this study thus does not imply the absence of soil moisture effects in the phase triplets.

A change of the structure function, i.e. the variation of the scatterers with depth, in the volume model could render the model more flexible with regards to the soil moisture sensitivities to account for their observed variability. It would e.g. enable the prediction of larger sensitivities: these are consistent with a large concentration of inhomogeneities deeper in the soil and less scattering from the upper parts, cf. the buried target of Morrison et al. (2013). The depth of the buried target governs the sensitivity of ϕ with respect to m_v. In natural soils, a layered soil could have a similar impact on the interferometric observables (Rabus et al., 2010). Also the variation of soil moisture with depth and the choice of dielectric mixing model are expected to impact the interferometric signals (De Zan et al., 2014; Rabus et al., 2010). A model combining surface dielectric effects and volume scattering could similarly account for some of the variability of the soil moisture effects across different fields.

7.3. Differences between polarizations

Even though the soil moisture impact is similar for HH, HV and VV, the differences between the polarizations can potentially provide further insight into the scattering physics that give rise to the m_v and vegetation effects. In particular the sizeable impact of Δm_v on the HV phase might seem surprising given that the soil contribution at this channel is

expected to be considerably smaller than at HH or VV. Such a dependence has also been found by Barrett et al. (2013) in C and L-band, but for the former with the opposite sign.

In the CanEx data set the $\beta_{\Delta m_v}$ for the phase ϕ at HH and VV are similar: their differences do not show a consistent pattern regarding their sign or size, and are significantly different from zero for only 14% of the samples; see Table S4. In the Agrisar campaign the phase coefficients tend to be larger for HH than for VV, but this difference is only significant at $\alpha = 0.05$ in 25% of the samples, cf. Fig. 8 and Table S3. These discrepancies appear to be related to the crop: the difference in both fit and magnitude is particularly pronounced for wheat (230, 250), the difference in location for barley (440) and partially also for rape (101,140). For maize HH and VV behave similarly, but there are marked differences between the subROIs. The linear model for ϕ is not accurate for sugar beet (102, 460) in any polarization. Note that all crops except the latter consist of dominantly vertically oriented scatterers, for which the interaction with electromagnetic waves is expected to be significantly stronger in the vertical than the horizontal polarization, as the horizontal extent of the scatterers is small compared to the wavelength except for mature maize. The increased interaction of the waves with vegetation in VV is consistent with smaller (i.e. larger magnitude) $\beta_{\Delta m_v}$ for the phase ϕ as well as the larger scatter observed in VV.

The reputed change in the effective propagation due to forward scattering in the vegetation affects the optical path (cf. Section 7.1.1), and this polarization dependence is evident in the slope term of ϕ with respect to Δb in Table S3. Its magnitude is expected to be larger for VV than HH for vertically oriented crops: empirically, this difference is significant at $\alpha = 0.05$ for 230 and 250 (both wheat) as well as 440 (barley) and for two samples in 101 (rape).

The coefficients for $|\gamma|$ barely depend on the choice of polarization in the two campaigns; note, however, that the decorrelation appears not to be dominated by soil moisture effects in the Agrisar campaign, cf. Section 7.1.2. The vegetation-related decorrelation is, however, not strongly polarization-dependent (Table S3) either.

7.4. Robustness to implementation

The assumptions pointed out in Section 5 – the choice of reference phase, the parameterization of the vegetation, the estimation of the autocorrelation and the normality of the error term – are shown in Section 6.4 to have only minor impacts on the overall patterns found using regression analysis. Noticeable changes do occur for particular fields, e.g. due to representing the vegetation by its height rather than its biomass or by using a different reference phase. These are, however, limited in both number and extent. The lack of sensitivity with respect to the error model in the ϕ regressions (for example with respect to the consideration of the autocorrelation) tallies with the rationale of referencing the phase with scatterers in close proximity, thus limiting the influence of unmodelled phase patterns. The conclusions drawn from the statistical analyses thus appear to be reasonably robust to these assumptions.

7.5. Relevance of the soil moisture effects

As radar interferometry is commonly applied to estimate displacements and elevations, a question regarding the impact of soil moisture changes arises: how do they affect the estimation of displacements and elevations? The two data sets exhibit phase excursions of up to $\frac{\pi}{2}$, e.g. in Fig. 7, and we attributed these to soil moisture effects due to their conspicuous dependence on Δm_v. Phases of this magnitude were associated with coherence magnitudes of 0.5–0.8, which are commonly considered adequate for differential interferometry (Crosetto, Monserrat, Cuevas, & Crippa, 2011; Ketelaar & Hanssen, 2003).

Such a value of $\phi = \frac{\pi}{2}$ corresponds to a displacement of 2–3 cm at L-band. This spuriously inferred movement is of similar or larger

magnitude than most geophysical deformation mechanisms commonly studied using DInSAR. Furthermore, it can occur on comparatively rapid time scales of minutes to days. Also the spatial scales at which these changes occur can in certain cases be comparable to those of the deformation processes. These soil moisture effects can thus potentially render such deformation analyses unreliable. However, many common processing systems avoid such areas by deriving the phase information from stable point-like scatterers, but there have been numerous approaches (e.g. (Berardino, Fornaro, Lanari, & Sansosti, 2002; Ferretti et al., 2011)) to include areas such as soil, that do not act as point-like targets. These algorithms commonly map the phase information of as many interferograms as possible to one time series with a fixed master scene. This mapping could only reduce the soil moisture signal significantly if the non-linear terms of the soil moisture dependence of ϕ dominated. Otherwise, if the linear components dominated as in many of the fields observed in this study, the soil moisture variations will be preserved in the phase time series, from which the displacements are inferred. These estimated deformations are commonly assumed to exhibit a particular temporal behaviour, such as a movement with a constant velocity (Berardino et al., 2002). Under such an assumption, the deformation estimate would only be impacted if the soil moisture variations corresponded to that particular temporal model.

In the estimation of elevations using repeat-pass interferometry, the impact of a soil moisture phase term of $\frac{\pi}{2}$ (assumed independent of the baseline) on the inferred height will depend on the baseline. More specifically, it will scale with the height of ambiguity $h_a = \frac{2\pi}{|\kappa_z|}$. This spurious elevation can be compared to the one due to phase noise: apart from areas where interferometry is hardly feasible due to decorrelation, the number of looks is generally chosen so that this phase noise is much smaller than $\frac{\pi}{2}$ (Bamler & Hartl, 1998). Thus the soil moisture effect can dominate the noise; it will also generally exhibit spatial patterns that can be related to the topography. Soil moisture variations can thus induce errors in the estimated elevation models that are both significant and relevant.

8. Conclusions

We conducted an empirical study of the soil moisture effects of DInSAR observables at L-band in a model-independent way. These analyses reveal that there is a dependence of the phase ϕ on changes in soil moisture Δm_v in both data sets examined. The decorrelation is also related to such changes; this relation is more pronounced in the CanEx data set, where the time difference between the acquisitions is smaller. The sign of the phase dependence and also its magnitude point towards volume scattering within the soil. This mechanism can also explain moisture-related decorrelation, and existing models could be adapted to capture the observed variabilities of the sensitivities with respect to soil moisture. The observed ϕ dependence on m_v is inconsistent with both the swelling soil and the penetration depth explanation.

These inferences only relate to the two L-band data sets analysed: their generality can only be established with additional studies. Future research might elucidate the impact of the soil characteristics (e.g. roughness or swelling behaviour), the properties of the vegetation cover, as well as the radar frequency. The wavelength governs the sensitivity to movements and roughness, as well as the penetration depth, which suggests a possible impact on the soil moisture effects. At higher frequencies such as X and Ku-band, temporal decorrelation is expected to be more pronounced. Frequent acquisitions, which can for example be made using ground-based radars, will thus be instrumental in providing the data that is necessary to improve the understanding and modelling of these effects.

Owing to the size of the observed phase values of up to $\phi = 0.5\pi$, corresponding to a displacement of 2–3 cm at L-band, these soil moisture effects deserve to be considered in repeat-pass InSAR studies. They have the potential to induce errors in the estimated deformations

in a wide range of temporal and spatial scales, thus indicating the importance of the study of these effects. Advances in the processing schemes and the physical modelling of these influences might lead to improvements in the estimates of the deformations and their uncertainties, thus contributing to the study of geophysical phenomena as diverse as tectonics, mass-movements and permafrost degradation.

Acknowledgements

Appendix A. Supplementary data

Supplementary data to this article can be found online at http://dx.doi.org/10.1016/j.rse.2015.04.012.

References

Bamler, R., & Hartl, P. (1998). Synthetic aperture radar interferometry. Inverse Problems, 14, 1–54.
Barrett, B., Whelan, P., & Dwyer, N. (2012). The use of C- and L-band repeat-pass interferometric SAR coherence for soil moisture change detection in vegetated areas. The Open Remote Sensing Journal, 5, 37–53.
Barrett, B., Whelan, P., & Dwyer, E. (2013). Detecting changes in surface soil moisture content using differential SAR interferometry DInSAR. International Journal of Remote Sensing, 34, 7091–7112.
Berardino, P., Fornaro, G., Lanari, R., & Sansosti, E. (2002). A new algorithm for surface deformation monitoring based on small baseline differential SAR interferograms. IEEE Transactions on Geoscience and Remote Sensing, 40, 2375–2383.
Cloude, S. R. (2009). Polarisation: Applications in remote sensing. Oxford University Press.
Cloude, S., & Papathanassiou, K. (1998). Polarimetric SAR interferometry. IEEE Transactions on Geoscience and Remote Sensing, 36, 1551–1565.
Crosetto, M., Monserrat, O., Cuevas, M., & Crippa, B. (2011). Spaceborne differential SAR interferometry: Data analysis tools for deformation measurement. Remote Sensing, 3, 305–318. http://dx.doi.org/10.3390/rs3020305 (URL: http://www.mdpi.com/2072-4292/3/2/305).
De Zan, F., Parizzi, A., Prats-Iraola, P., & Lopez-Dekker, P. (2014). A SAR interferometric model for soil moisture. IEEE Transactions on Geoscience and Remote Sensing, 52, 418–425.
Emardson, T., Simons, M., & Webb, F. H. (2003). Neutral atmospheric delay in interferometric synthetic aperture radar applications: Statistical description and mitigation. Journal of Geophysical Research, 108, 2231.
Ferretti, A., Fumagalli, A., Novali, F., Prati, C., Rocca, F., & Rucci, A. (2011). A new algorithm for processing interferometric data-stacks: SqueeSAR. IEEE Transactions on Geoscience and Remote Sensing, 49, 3460–3470. http://dx.doi.org/10.1109/TGRS.2011.2124465.
Gabriel, A., Goldstein, R., & Zebker, H. (1989). Mapping small elevation changes over large areas: Differential radar interferometry. Journal of Geophysical Research, 94, 9183–9191.
Galloway, D., & Hoffmann, J. (2007). The application of satellite differential SAR interferometry-derived ground displacements in hydrogeology. Hydrogeology Journal, 15, 133–154.
German Aerospace Center (2008). AGRISAR 2006. Final report. Technical report. Microwaves and Radar Institute (URL: http://earth.esa.int/campaigns/DOC/AGRISAR_Final_Report.pdf).
Goldstein, R. M. (1995). Atmospheric limitations to repeat-track radar interferometry. Geophysical Research Letters, 22, 2517–2520.
Hajnsek, I., & Prats, P. (2008). Soil moisture estimation in time with D-InSAR. Proc. IGARSS 2008 (pp. 546–549).
Hallikainen, M., Ulaby, F., Dobson, M., El-Rayes, M., & Wu, L. K. (1985). Microwave dielectric behavior of wet soil — Part 1: Empirical models and experimental observations. IEEE Transactions on Geoscience and Remote Sensing, 23, 25–34.
Hamadi, A., Albinet, C., Borderies, P., Koleck, T., Villard, L., Ho Tong Minh, D., et al. (2014). Temporal survey of polarimetric P-band scattering of tropical forests. IEEE Transactions on Geoscience and Remote Sensing, 52, 4539–4547. http://dx.doi.org/10.1109/TGRS.2013.2282357.
Hamadi, A., Borderies, P., Albinet, C., Koleck, T., Villard, L., Ho Tong Minh, D., et al. (2014). b. Temporal coherence of tropical forests at P-band: Dry and rainy seasons. IEEE Geoscience and Remote Sensing Letters, 12, 557–561. http://dx.doi.org/10.1109/LGRS.2014.2350513.
Hanssen, R. (2001). Radar interferometry: Data interpretation and analysis. Kluwer Acad.
Hensley, S., Michel, T., van Zyl, J., Muellerschoen, R., Chapman, B., Oveisgharan, S., et al. (2011). Effect of soil moisture on polarimetric-interferometric repeat pass observations by UAVSAR during 2010 Canadian soil moisture campaign. Proceedings of IGARSS 2011 (pp. 1063–1066).
Ishimaru, A. (1997). Wave propagation and scattering in random media. IEEE Press.

Jones, C., & Davis, B. (2011). High resolution radar for response and recovery: Monitoring containment booms in Barataria Bay. Photogrammetric Engineering & Remote Sensing, 77, 102–105.
Judge, G., Hill, R., Griffiths, W., Lutkepohl, H., & Lee, T. (1983). Introduction to the theory and practice of econometrics. John Wiley & Sons.
Kampes, B. (2006). Radar interferometry: Persistent scatterer technique. Springer.
Ketelaar, V., & Hanssen, R. (2003). Separation of different deformation regimes using PS-InSAR data. Proc. of FRINGE 2003 Workshop, Frascati, Italy.
Koenker, R. (2005). Quantile regression. Cambridge University Press.
Koenker, R. (2013). Quantreg: Quantile regression. URL: http://CRAN.R-project.org/package=quantreg (r package version 4.98)
Lavalle, M., Simard, M., & Hensley, S. (2012). A temporal decorrelation model for polarimetric radar interferometers. IEEE Transactions on Geoscience and Remote Sensing, 50, 2880–2888. http://dx.doi.org/10.1109/TGRS.2011.2174367.
Liu, L., Zhang, T., & Wahr, J. (2010). InSAR measurements of surface deformation over permafrost on the North Slope of Alaska. Journal of Geophysical Research, 115, F03023.
Magagi, R., Berg, A., Goita, K., Belair, S., Jackson, T., Toth, B., et al. (2013). Canadian experiment for soil moisture in 2010 (CanEx-SM10): Overview and preliminary results. IEEE Transactions on Geoscience and Remote Sensing, 51, 347–363. http://dx.doi.org/10.1109/TGRS.2012.2198920.
Massonnet, D., Briole, P., & Arnaud, A. (1995). Deflation of Mount Etna monitored by spaceborne radar interferometry. Nature, 375, 567–570. http://dx.doi.org/10.1038/375567a0.
Massonnet, D., Rossi, M., Carmona, C., Adragna, F., Peltzer, G., Feigl, K., et al. (1993). The displacement field of the Landers earthquake mapped by radar interferometry. Nature, 364, 138–142. http://dx.doi.org/10.1038/364138a0.
Mironov, V., Kerr, Y., Wigneron, J. P., Kosolapova, L., & Demontoux, F. (2013). Temperature- and texture-dependent dielectric model for moist soils at 1.4 GHz. IEEE Geoscience and Remote Sensing Letters, 10, 419–423. http://dx.doi.org/10.1109/LGRS.2012.2207878.
Mitchell, A. (1991). Soil surface shrinkage to estimate profile soil water. Irrigation Science, 12, 1–6.
Monnier, J. D. (2007). Phases in interferometry. New Astronomy Reviews, 51, 604–616. http://dx.doi.org/10.1016/j.newar.2007.06.006 (URL: http://www.sciencedirect.com/science/article/pii/S1387647307000656).
Moore, D., & Singer, M. (1990). Crust formation effect on soil erosion processes. Soil Science Society of America Journal, 54, 1117–1123.
Morrison, K., Bennett, J., & Nolan, M. (2013). Using DInSAR to separate surface and subsurface features. IEEE Transactions on Geoscience and Remote Sensing, 51, 3424–3430.
Morrison, K., Bennett, J., Nolan, M., & Menon, R. (2011). Laboratory measurement of the DInSAR response to spatiotemporal variations in soil moisture. IEEE Transactions on Geoscience and Remote Sensing, 49, 3815–3823.
Nesti, G., Tarchi, D., Despan, D., Rudant, J. P., Bedidi, A., Borderies, P., et al. (1998). Phase shift and decorrelation of radar signal related to soil moisture changes. Proc. of 2nd International Workshop on Retrieval of Bio-Geo-physical Parameter from SAR data for Land Applications (pp. 21–23).
Nolan, M. (2003a). DInSAR measurement of soil moisture. IEEE Transactions on Geoscience and Remote Sensing, 41, 2802–2813.
Nolan, M. (2003b). Penetration depth as a DInSAR observable and proxy for soil moisture. IEEE Transactions on Geoscience and Remote Sensing, 41, 532–537.
Norrish, K. (1954). The swelling of montmorillonite. Discussions of the Faraday Society, 18, 120–134.
Peplinski, N. R., Ulaby, F. T., & Dobson, M. C. (1995). Dielectric properties of soils in the 0.3–1.3-GHz range. IEEE Transactions on Geoscience and Remote Sensing, 33, 803–807.
Pinheiro, J. C., & Bates, D. M. (2000). Mixed-effect models in S and S-PLUS. Springer.
Pinheiro, J., Bates, D., DebRoy, S., Sarkar, D., & R Core Team (2013). nlme: Linear and nonlinear mixed effects models. 1–108 (R package version 3.1-108).
Rabus, B., Wehn, H., & Nolan, M. (2010). The importance of soil moisture and soil structure for InSAR phase and backscatter, as determined by FDTD modeling. IEEE Transactions on Geoscience and Remote Sensing, 48, 2421–2429.
Rosen, P., Hensley, S., Joughin, I., Li, F., Madsen, S., Rodriguez, E., et al. (2000). Synthetic aperture radar interferometry. Proceedings of the IEEE, 88, 333–382.
Rudant, J. P., Bedidi, A., Calonne, R., Massonnet, D., Nesti, G., & Tarchi, D. (1996). Laboratory experiment for the interpretation of phase shift in SAR interferograms. Proceedings of FRINGE.
Srivastava, S. K., & Jayaraman, V. (2001). Relating interferometric signature of repeat pass ERS-1 SAR signals to dynamic land cover changes. Acta Astronautica, 48, 37–44.
te Brake, B., Hanssen, R., van der Ploeg, M., & de Rooij, G. (2013). Satellite based radar interferometry to estimate large-scale soil water depletion from clay shrinkage: Possibilities and limitations. Vadose Zone Journal, 12. http://dx.doi.org/10.2136/vzj2012.0098.
Tsang, L., Kong, J. A., & Ding, K. H. (2000). Scattering of electromagnetic waves: Theories and applications. John Wiley & Sons.
Ulaby, F., Tavakoli, A., & Senior, T. (1987). Microwave propagation constant for a vegetation canopy with vertical stalks. IEEE Transactions on Geoscience and Remote Sensing, 25, 714–725.
Weydahl, D. J. (2001). Analysis of ERS SAR coherence images acquired over vegetated areas and urban features. International Journal of Remote Sensing, 22, 2811–2830. http://dx.doi.org/10.1080/01431160010006412.
Yin, Q., Hong, W., Li, Y., & Lin, Y. (2014). Analysis on soil moisture estimation of SAR data based on coherent scattering model. EUSAR.
Zebker, H., & Villasenor, J. (1992). Decorrelation in interferometric radar echoes. IEEE Transactions on Geoscience and Remote Sensing, 30, 950–959.
Zwieback, S., & Hajnsek, I. (2014). Statistical tests for symmetries in polarimetric scattering coherency matrices. IEEE Geoscience and Remote Sensing Letters, 11, 308–312.